Supporting Information

NanoStructured Tin Catalysts for Selective Electrochemical Reduction of Carbon Dioxide to Formate

Sheng Zhang, Peng Kang, Thomas J. Meyer*

Department of Chemistry, University of North Carolina at Chapel Hill, Chapel Hill, NC 27599, USA. E-mail: tjmeyer@unc.edu

Experimental section

1 Materials preparation

Preparation of nano tin oxide catalysts. Tin oxide nanoparticles were synthesized by a modification of a facile hydrothermal method.[1] The appropriate amount of Tin(II) chloride ($SnCl_2$, 98%, Acros Organics) precursor was dissolved in ethylene glycol (EG, Fisher Scientific) with trace amount of water, mixed with appropriate amount of carbon support (carbon black, VULCAN® XC72, purchased from Cabot Corporation; or graphene prepared by a thermal expansion method reported in the literature[2]), and then ultrasonicated for ~30 min. The resulting mixture was heated up to 196 ^{o}C and then refluxed with vigorous stirring. The product was collected by ultrafiltration and washed with deionized water, and then dried for 3 h at 90 ^{o}C in vacuum. Particle size of the resultant tin oxide can be tuned by reaction time. When reaction time proceeded in 30 min, about 3 nm tin oxide nanoparticles were formed. Around 5 nm tin oxide nanoparticles were obtained when the reaction time was increased to 3 hours. The largest tin oxide nanoparticles prepared here were about 10 nm after 6 hours.

Electrodeposited tin particles on pre-polished glassy carbon electrode. A glassy carbon electrode was first well polished in 0.3 and 0.05 micro Alumina powder to obtain a mirror surface and then sonicated and thoroughly rinsed with Milli-Q water and acetone. The polished glassy carbon electrode as the working electrode was immersed into 10 mM $SnCl_2$ dissolved acetonitrile with 0.1 M $TBAPF_6$ electrolyte, and then was scanned for 5 cycles from -1 to -2 V *verse* SCE. Based on CV curves described above, about 0.2 C of charge was consumed during the reduction of $SnCl_2$ to Sn(0) giving the loading of electrodeposited Sn on glassy carbon to be about 123 μg.

Tin foil. Commercial tin foil (1.7 g/50×50 mm), 0.25 mm (0.01 in) thick, 99.998% (metals basis) was purchased from Alfa Aesar. Before electrochemical measurements, the as-received tin foil (about 3400 μg) was pretreated in 1 M HNO_3 for 10 second to remove surface oxide and contaminants.[3]

2 Electrochemical measurements

The electrochemical measurements were carried out in a gas-tight two compartment electrochemical cell system controlled with a CHI601 D station (CH Instruments, Inc., USA)

with Pt wire and Saturated Calomel Reference Electrode (SCE) as the counter electrode and reference electrode, respectively. The working electrodes were prepared by loading sample suspension onto the prepolished glass carbon electrodes. In brief, as prepared *nano*-SnO_2/carbon black or *nano*-SnO_2/graphene sample was dispersed in ethanol and ultrasonicated for 15 min to form a uniform catalyst suspension (2 mg mL^{-1}). A total of 7.5 μL of well dispersed catalyst ink was applied onto the pre-polished glassy carbon electrode (3 mm in diameter). This gives the loading of carbon supported *nano*-SnO_2 sample to be about 15 μg, and the amount of Sn is calculated to be about 3.45μg based on the *nano*-SnO_2 content of ~30% in catalyst. After drying at room temperature, 5 μL of 0.05 wt% Nafion solution was applied onto the surface of the catalyst layer to form a thin protective film. The well-prepared electrodes were dried at room temperature overnight before the electrochemical tests. Linear sweep voltammetric (LSV) scans were recorded in N_2 or CO_2 saturated 0.1 M $NaHCO_3$, while controlled potential electrolysis was performed in 0.1 M $NaHCO_3$ electrolyte with CO_2 flow.

3 Physical characterizations

Raman spectra were collected by Raman measurments (Renishaw) with a 514 nm laser. X-ray diffraction (XRD) data were collected on Bruker Smart APEX II CCD diffractometer equipped with Cu-target X-ray tube and operated at 1600 watts. High-resolution TEM (HRTEM) was obtained on a JEOL 2010F-FasTEM. Scanning electron microscopy (SEM) and energy dispersive X-ray spectrometer (EDS) were obtained on on a FEI Helios 600 Nanolab Dual Beam System focused ion beam (FIB) equipped with an Oxford Instruments, INCA PentaFET−x3 X-ray detector with the electron beam set to 20 keV and a beam current of 0.69 nA. In addition, the ion beam was used to mill into the film and determine its permeability to the deposited metal particles. EDS measurements were made of film surfaces, and with a 1 $μm^2$, 100 nm deep square milled into the film, another EDS spectrum was recorded.

NMR analysis was used to quantify the yield of formate during controlled potential electrolysis. NMR spectra were recorded on Bruker NMR spectrometers (AVANCE-400). 1H NMR spectra were referenced to residual solvent signals. At the end of electrolysis periods, gaseous samples (0.8 ml) were drawn from the headspace by a gas-tight syringe (Vici) and injected into the GC (Varian 450-GC, pulsed discharge helium ionization detector, PDHID). Calibration curves for H_2 and CO were determined separately.

X-ray photoelectron spectra (XPS) were obtained at the Chapel Hill Analytical and Nanofabrication Lab (CHANL) at UNC. A Kratos Analytical Axis UltraDLD spectrometer with monochromatized X-ray Al Kα radiation (1486.6 eV) with an analysis area of 1 mm^2 was used. A survey scan was first performed with a step size of 1 eV, a pass energy of 80 eV, and a dwell time of 200 ms. High resolution scans were then taken for each element present with a step size of 0.1 eV and a pass energy of 20 eV. The binding energy for all peaks was referenced to the C 1s peak at 284.6 eV.
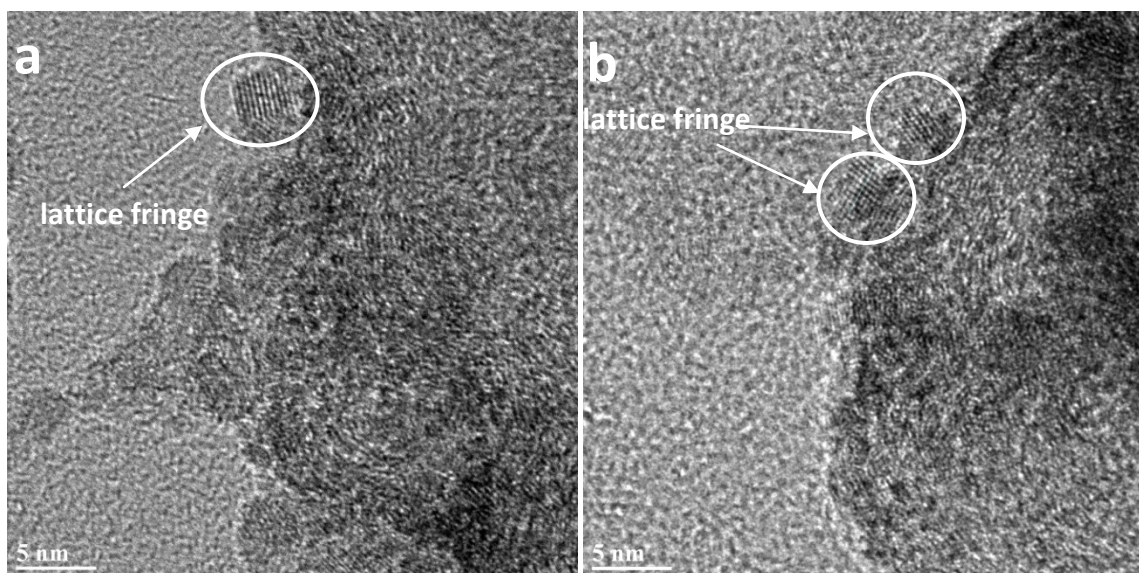
Figure S1 High resolution TEM images for tin oxide nanoparticles on carbon black. The average lattice spacing for these tin oxide nanoparticles was calculated to be ~0.335 nm, which correspond to the (110) planes of rutile SnO_2.[4,5]
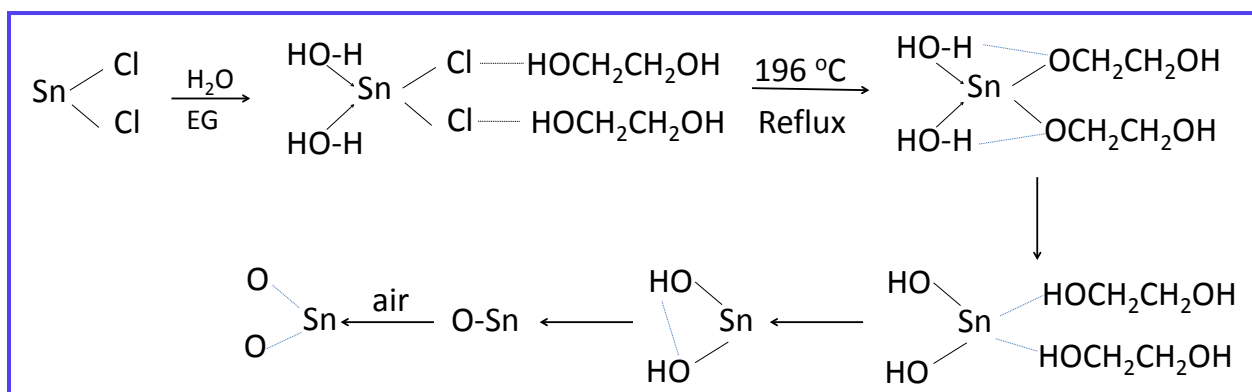
Figure S2 Schematic illustration of a proposed mechanism responsible for the formation of SnO$_2$ nanoparticles by hydrothermal method. It features prior coordination to the SnCl$_2$ precursor by ethylene glycol (EG) and water with displacement of Cl$^-$. At high temperatures aquated Sn(II) forms Sn(OH)$_2$ which is decomposed into SnO and further oxidized by oxygen in the air into SnO$_2$ nanoparticles.
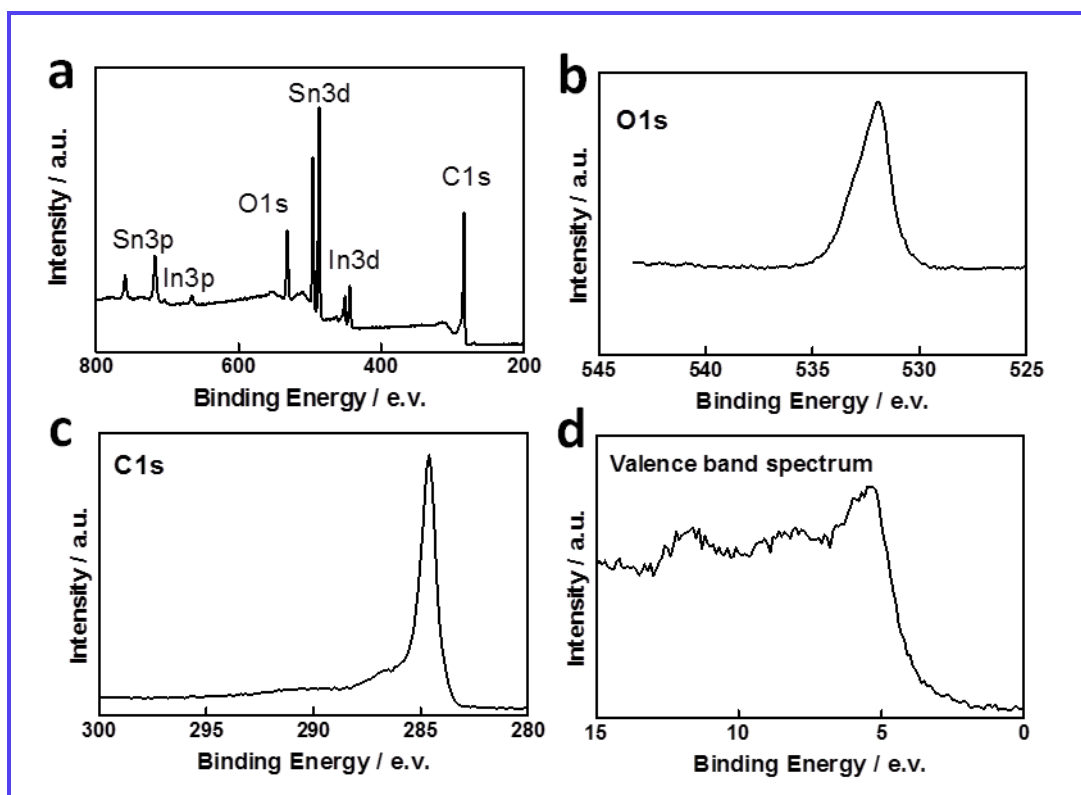
Figure S3 Physical characterization of *nano*-SnO$_2$/carbon black sample: (a) survey X-ray photoelectron spectroscopy (XPS) spectrum; high resolution O1s XPS spectrum (b), C 1s spectrum (c), and valence band (d). Figure S3a shows the survey XPS spectrum for *nano*-SnO$_2$/carbon black. The peaks can be assigned to the elements of Sn, In, C, and O, where the presence of element In is due to the background. In the high resolution XPS valence band spectrum in Figure S3d, three binding energies appear above 5 eV consistent with SnO$_2$ with two binding energies anticipated for Sn metal and four for SnO.[6]
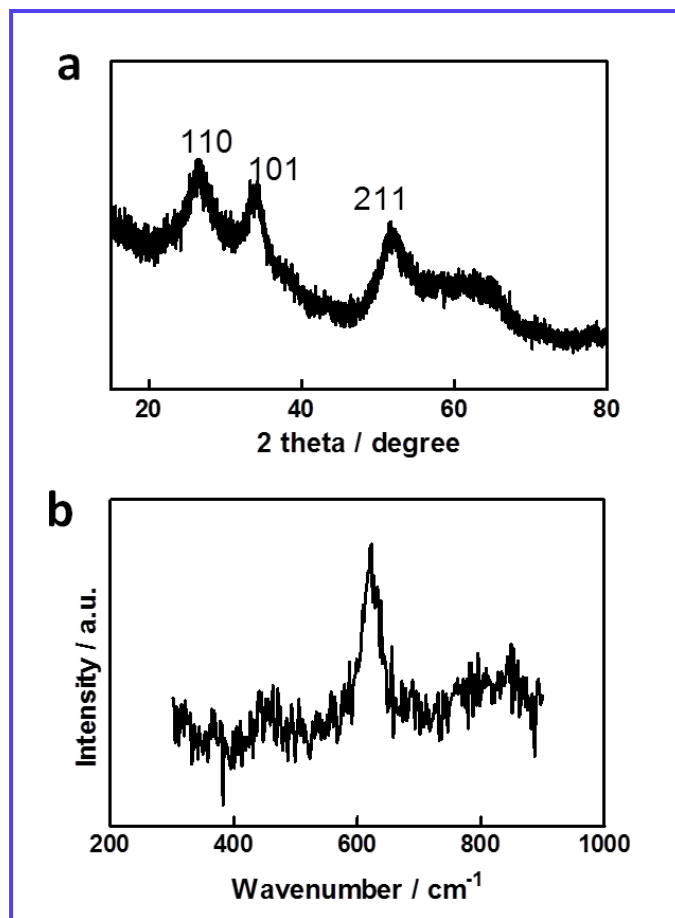
Figure S4 XRD pattern (a) and enlarged scattering Raman spectrum (b) of *nano*-SnO$_2$ on carbon black. The average particle size of the SnO$_2$ nanocrystals can be calculated by using the Scherrer equation, eq 1:

$$L = \frac{0.9\lambda_{K\alpha 1}}{B_{2\theta}\cos\theta_{max}} \tag{1}$$

In this equation, L is the mean particle size, $\lambda_{K\alpha 1}$ is the X-ray wavelength (λ=1.5418 Å), θmax is the angle for the (110) plane, and $B_{2\theta}$ is the band width at half height for the Pt(110) plane. The XRD patterns are noisy in appearance due to the presence of carbon support. To get a more accurate value of nano-SnO$_2$ particle size, these patterns had been smoothed using Gaussian Fitting before the average particle sizes of nano SnO$_2$ were calculated based on the Scherrer equation. Based on this analysis, the SnO$_2$ volume averaged diameter from the XRD data was ~4.8 nm which is slightly less than the calculated volume area average diameters from TEM. The discrepancy probably arises from the fact that SnO$_2$ nanoparticles (smaller than 1 nm) are poorly shown in TEM images. If included, they would decrease the averaged diameters from TEM images.[7]
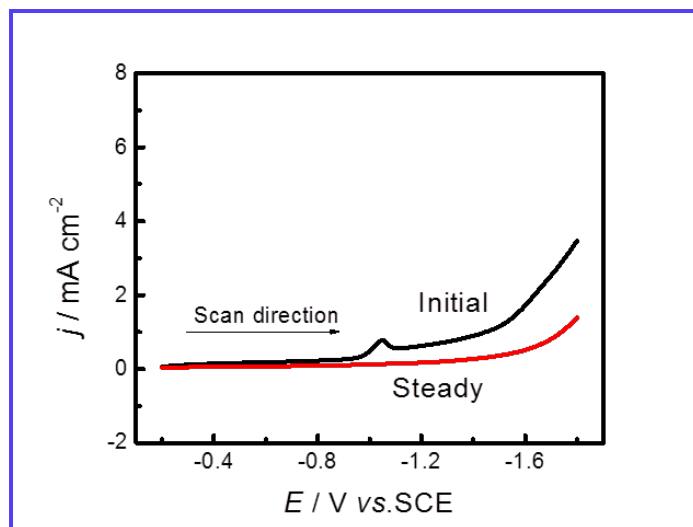
Figure S5 Initial and steady single reductive linear sweep voltammetric (LSV) scans of *nano* SnO_2/carbon black in N_2 saturated 0.1 M $NaHCO_3$ at the scanning rate of 50 mV s^{-1}. In the LSV curves, a reduction peak appears at -1.0 V in initial scan. It arises from reduction of SnO_2 nanoparticles[8] and disappears after 50 cyclic voltammetry (CV) cycles from -1 to -1.8 V indicative of reductive saturation on carbon black. All the LSV scans and controlled potential electrolysis in our report were recorded at reduced *nano* tin oxide. A small amount of tin oxide might still persist within the core of the reduced Sn catalyst. However, due to lack of access to electrolyte, the residual tin oxide presumably does not contribute to CO_2 reduction.
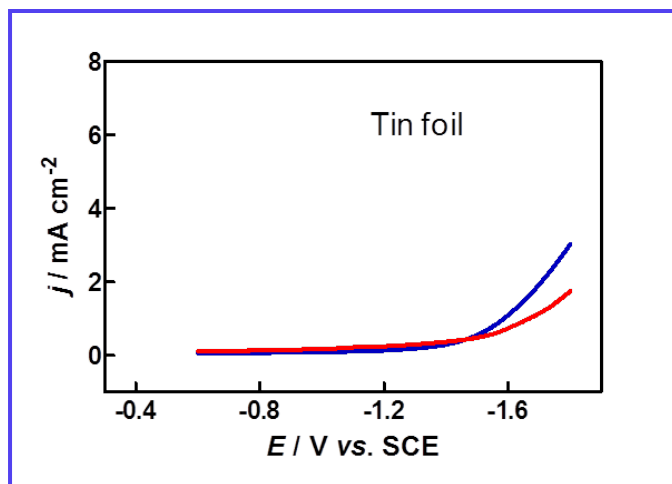
Figure S6 Single reductive linear sweep voltammetric (LSV) scans with scan rate of 50 mV s^{-1} at tin foil under N_2 (in red) and CO_2 (in blue) saturated 0.1 M $NaHCO_3$ solution. The current density at -1.8 V was about 3.2 mA cm^{-2} and the corresponding specific current density was about 0.05 A g^{-1}. Prior to electrochemical measurements, tin foil was pretreated in 1 M HNO_3 for 30 s to remove surface contaminants.
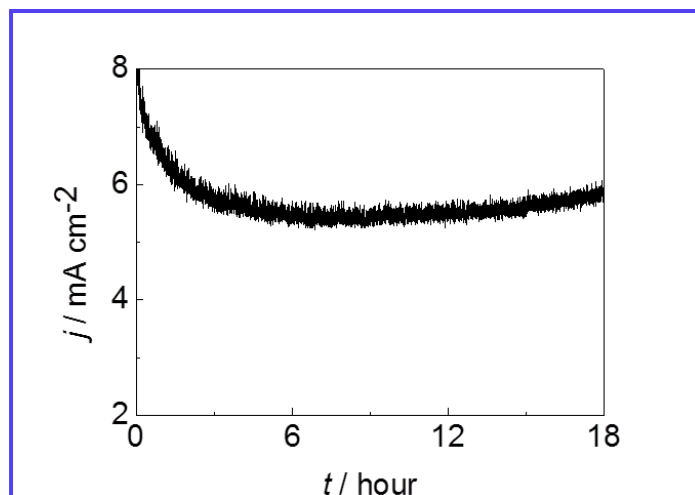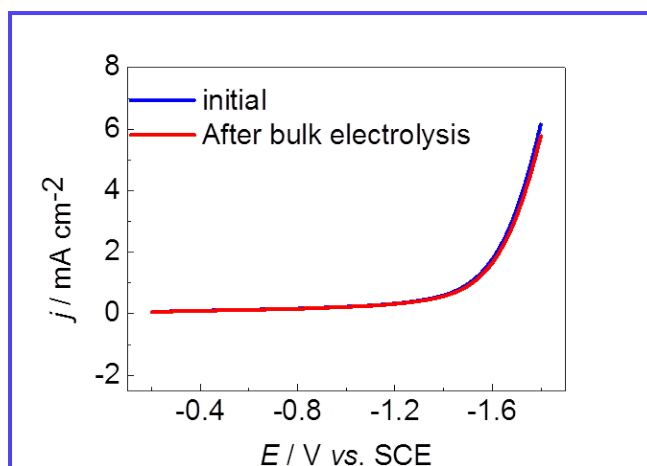
Figure S7 Controlled potential electrolysis at -1.8 *verse* SCE at *nano*-SnO$_2$/carbon black sample in 0.1 M NaHCO$_3$ solution with CO$_2$ flow. Controlled potential electrolysis at *nano* SnO$_2$/carbon black at -1.8 V resulted in a steady state catalytic current density of ca. 5.4 mA cm^{-2}.
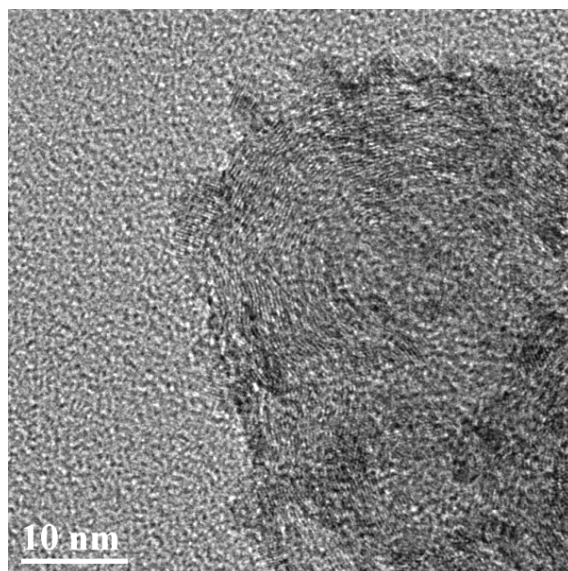
Figure S8 TEM images of *nano* SnO$_2$/carbon black after controlled potential electrolysis, which showed the morphology of *nano* SnO$_2$/carbon black was essentially unchanged compared with the initial *nano* SnO$_2$/carbon black sample.

Figure S9 Single reductive LSV scans at *nano* SnO_2/carbon black sample before and after bulk electrolysis, which showed the catalytic property of *nano*-SnO_2/carbon black was essentially unchanged after controlled potential electrolysis.
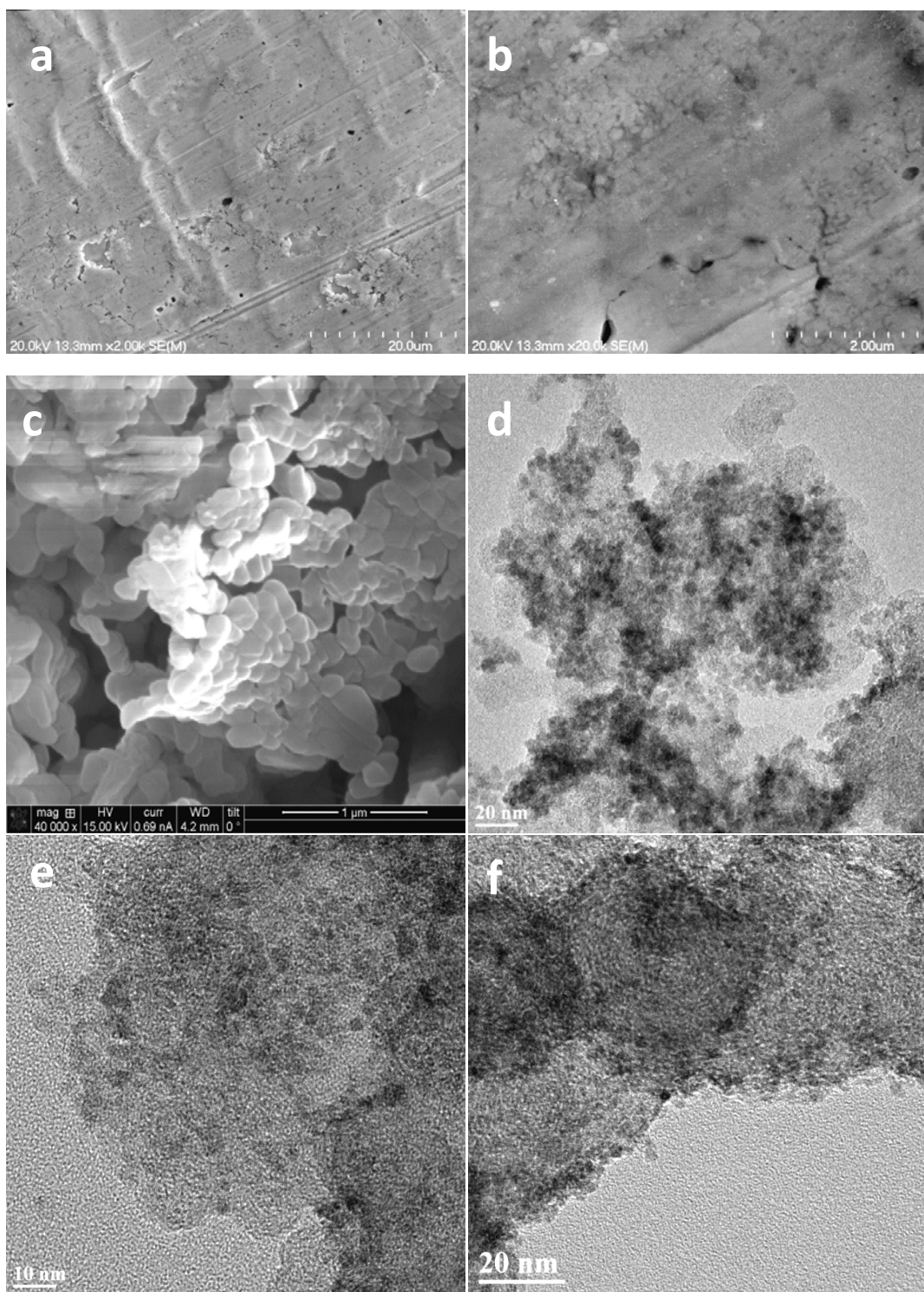
Figure S10 SEM images of Sn foil (a, b); SEM image of 200 nm Sn nanoparticles prepared by electrochemical reduction (c); TEM image of 10 nm SnO_2 nanoparticles on carbon black(d); TEM image of 5 nm SnO_2 nanoparticles on carbon black (e); and TEM image of 3 nm SnO_2 nanoparticles on carbon black(f). The particle sizes of *nano*-SnO_2 were tuned through reaction time (see Materials preparation).
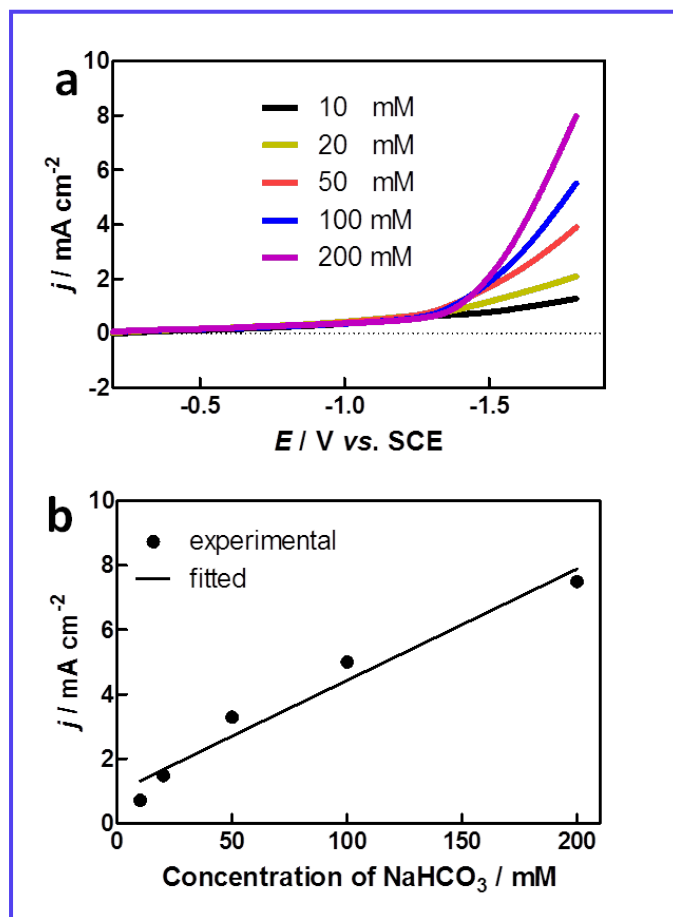
Figure S11 Single reductive LSV scans (a) at 5 nm reduced tin oxide catalyst in different concentrated CO_2 saturated $NaHCO_3$ electrolyte, where total concentration of Na^+ was kept at 0.2 M by adding $NaClO_4$. Under these conditions, $NaHCO_3/CO_2$ is the buffer. The pH values slightly increased from 6.2 to 6.9 when the $NaHCO_3$ concentrations were increased from 10 mM to 200 mM. Without any $NaHCO_3$, the pH is ca. 5.5 under 1 atm of CO_2. $NaHCO_3$ concentration dependence (b) of current density at -1.8 V, which showed catalytic current densities for CO_2 reduction nearly linearly increase with concentrations of HCO_3^- in the electrolyte. We propose that HCO_3^- is the likely source as the dominant proton donor based on its *pK*a value (10.33) compared to water (15.7). Carbonic acid in the CO_2 saturated solutions is present but in small amount. Additional evidence is provided by the Tafel slope in (Figure S12) of ~70 mV dec^{-1}, which is close to 59 mV dec^{-1}. This suggests a mechanism involving a rate-determining chemical step[9]. These kinetics are consistent with electron transfer and adsorption of $CO_2^{\cdot-}$ followed by rate limiting proton transfer from HCO_3^-.
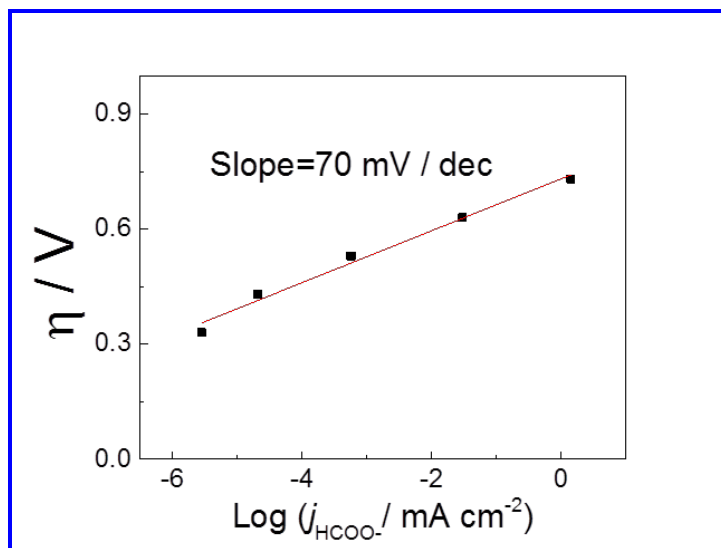
Figure S12 Tafel plot for production of formate at 5 nm SnO_2 sample based on the data in Figure 3, for production of formate at 5 nm SnO_2. The Tafel slope was calculated to be about 70 mV dec^{-1}, which is close to 59 mV dec^{-1}. This suggests a mechanism involving a chemical rate-determining step rather than an initial rate-determining transfer of one electron to CO_2.[9] This observation supports our proposed mechanism: equation 3, with protonation of $CO_2^{\cdot-}$ as the rate-determining step (RDS) during CO_2 reduction to formate at the nano SnO_2 catalyst.
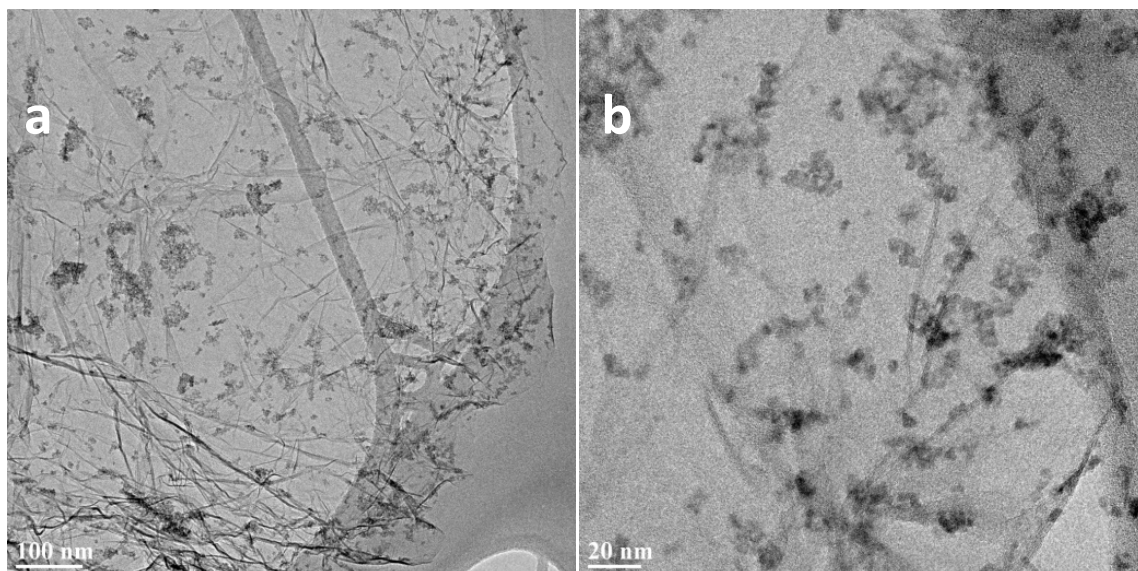
Figure S13 TEM images of *nano*-SnO$_2$/graphene sample, which showed SnO$_2$ nanoparticles with of ~5 nm diameter that are uniformly loaded on the surface of graphene. In contrast to the monodisperse SnO$_2$ nanoparticles in SnO$_2$/carbon black, there is an increase in the interconnections between SnO$_2$ nanoparticles to form SnO$_2$ nanoparticle clusters in the SnO$_2$/graphene samples. This may be due to the higher content of oxygen-containing defects in graphene used in this study (~8 at. % determined by XPS) than that in carbon black (~1 at. %).
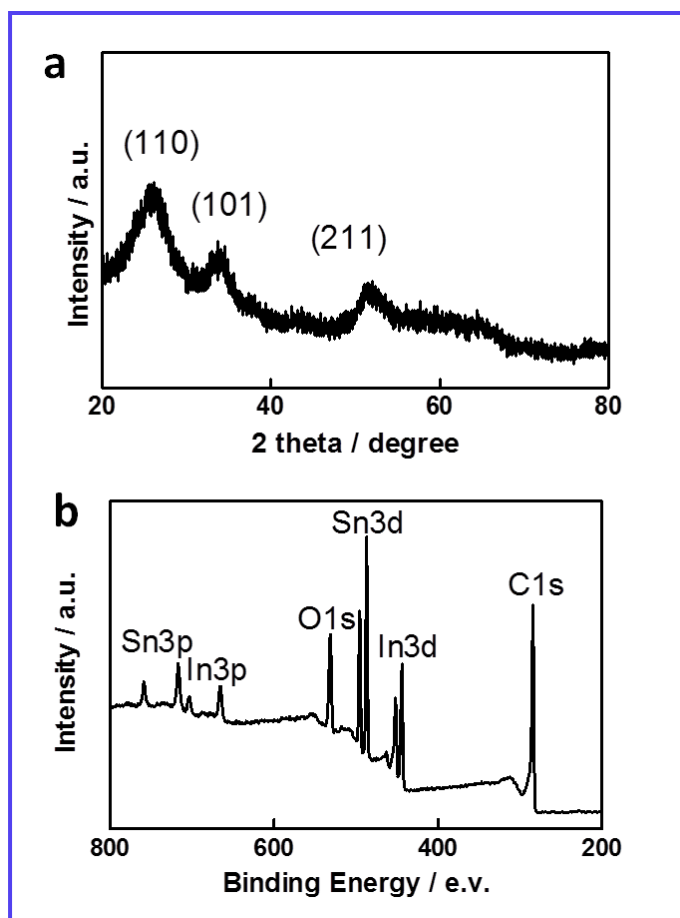
Figure S14 XRD (a) and survey XPS spectra(b) of *nano*-SnO$_2$/graphene sample. three intense diffraction peaks in the XRD pattern shown in Figure S4 at 2θ=25.6, 32.8, and 50.9 degrees can be indexed as the (110), (101), and (211) planes of the polycrystalline rutile SnO$_2$ structure, respectively. The XRD patterns are noisy in appearance due to the presence of carbon support. To get a more accurate value of nano-SnO$_2$ particle size, these patterns had been smoothed using Gaussian Fitting before the average particle sizes of nano SnO$_2$ were calculated based on the Scherrer equation. The average particle size of the SnO$_2$ nanocrystals on graphene can be calculated by using the Scherrer equation to be ~4.9 nm. In the survey XPS spectrum, these peaks can be assigned to the elements of Sn, In, C, and O, where the presence of element In is due to the background.
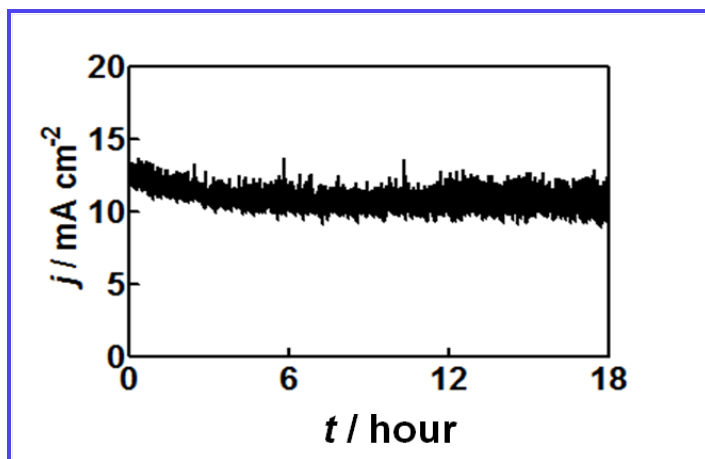
Figure S15 Controlled potential electrolysis at -1.8 *vs*. SCE at the reduced *nano*-SnO$_2$/graphene in 0.1 M NaHCO$_3$ solution with CO$_2$ flow. The reduced nano-SnO$_2$/graphene reaches higher Faradaic efficiencies for formate production (93.6%) at nearly twice the current density (10.2 mA cm^{-2}) as at SnO$_2$/carbon black.

Table S1 Faradaic efficiencies for formate over Sn catalysts from controlled potential electrolyses.

Faradaic efficiencies for formate	3 nm SnO$_2$	5 nm SnO$_2$	10 nm SnO$_2$	Electrodeposited 200 nm Sn nanoparticles	Sn foil
-1.6 V	40	51	41	29	20
-1.8 V	64	86	60	35	28
-2.0 V	33	39	32	26	18

References

(1) Jiang, L.; Sun, G.; Zhou, Z.; Sun, S.; Wang, Q.; Yan, S.; Li, H.; Tian, J.; Guo, J.; Zhou, B.; Xin, Q. *J. Phys. Chem. B* **2005**, *109*, 8774.

(2) McAllister, M. J.; Li, J. L.; Adamson, D. H.; Schniepp, H. C.; Abdala, A. A.; Liu, J.; Herrera-Alonso, M.; Milius, D. L.; Car, R.; Prud'homme, R. K.; Aksay, I. A. *Chem. Mater.* **2007**, *19*, 4396.

(3) Wu, J. J.; Risalvato, F. G.; Ke, F. S.; Pellechia, P. J.; Zhou, X. D. *J. Electrochem. Soc.* **2012**, *159*, F353.

(4) Wang, D.; Kou, R.; Choi, D.; Yang, Z.; Nie, Z.; Li, J.; Saraf, L. V.; Hu, D.; Zhang, J.; Graff, G. L.; Liu, J.; Pope, M. A.; Aksay, I. A. *ACS Nano* **2010**, *4*, 1587.

(5) Zhang, D. F.; Sun, L. D.; Yin, J. L.; Yan, C. H. *Adv. Mater.* **2003**, *15*, 1022.

(6) Kover, L.; Moretti, G.; Kovacs, Z.; Sanjines, R.; Csemy, I.; Margaritondo, G.; Palinkas, J.; Adachi, H. *J. Vac. Sci. Technol. A.* **1995**, *13*, 1382.

(7) Zhang, S.; Shao, Y. Y.; Yin, G. P.; Lin, Y. H. *J. Mater. Chem.* **2009**, *19*, 7995.

(8) Nakayama, S.; Sugihara, T.; Matsumoto, J.; Notoya, T.; Osakai, T. *J. Electrochem. Soc.* **2011**, *158*, C341.

(9) Chen, Y.; Kanan, M. W. *J. Am. Chem. Soc.* **2012**, *134*, 1986.